CHIN. PHYS. LETT. Vol. 33, No. 7 (2016) 077101

Phase Transition and Band Structure Tuned by Strains in $Al_{1/2}Ga_{1/2}N$ Alloy of Complex Structure *

Li-Xia Qin(秦丽霞)[1**], Rong-Li Jiang(蒋荣立)[2]

[1]*Department of Physics and College of Chemical Engineering, China University of Mining and Technology, Xuzhou 221116*

[2]*College of Chemical Engineering, China University of Mining and Technology, Xuzhou 221116*

(Received 1 April 2016)

Phase transition and band structure tuned by uniaxial and biaxial strains are systematically investigated based on the density-functional theory for ordered $Al_{1/2}Ga_{1/2}N$ alloys of complex structures. Although the structural transformations to graphite-like from wurtzite are energetically favorable for both types of strain, the phase transitions are different in nature: the second-order transition induced by uniaxial strain is jointly driven by the mechanical and dynamical instabilities and the first-order transition by biaxial strain only by the mechanical instability. The wurtzite phase always shows the direct band gap, while the band gap of the graphite-like phase is always indirect. Furthermore, the band gaps of the wurtzite phase can be reduced by both types of strain, while that of the graphite-like phase is enhanced by uniaxial strain and is suppressed by biaxial strain.

PACS: 71.22.+i, 62.10.+s, 63.20.D− DOI: 10.1088/0256-307X/33/7/077101

Ground-state AlN and GaN are in the wurtzite structure, which have been investigated extensively owing to their abundant physics and technological applications.[1,2] Since the band gap (E_g) is sensitive to the change in structural details, strain engineering has been widely adopted to tune electronic structures to satisfy particular practical applications in the optoelectronic field.[3–5] An intermediate structure between wurtzite and rock salt phases has been theoretically reported:[6,7] the graphite-like phase is fivefold coordinated and belongs to hexagonal symmetry. The structural evolution from wurtzite to graphite-like and band structures has been investigated in detail for AlN and GaN to achieve the desired electronic properties.[8–11] Such phase transitions are different in nature for both types of strain with different mechanisms.[12] When AlGaN alloys are epitaxially grown on AlN and GaN substrates, E_g varies from 3.20 eV to 6.14 eV with concentration.[13,14] Furthermore, E_g of alloy on AlN substrates is always larger than that of alloy on GaN at given concentration, which indicates that compressive biaxial strain enhances E_g more drastically than tensile biaxial strain. Recently, phase transition and band structure have been systematically studied to show the strain-induced novel properties for $Al_{1/2}Ga_{1/2}N$ alloy via first-principles calculations.[15] The ordered alloys are based on $2\times2\times1$ supercells: two AlN cells are along the [110] direction and two GaN ones along the $[\bar{1}10]$ direction. However, it is difficult to retain hexagonal symmetry, since the Al(Ga)–N bonds, characterized by the internal parameter u, are not strictly along the c-axis due to the difference in chemical environments. Therefore, more complex structures should be adopted to describe the ordered hexagonal AlGaN alloys, thus to enhance the reliability of simulations.

In this Letter, our aim is to systematically investigate the effects of strain on the phase transition and band structure of $Al_{1/2}Ga_{1/2}N$ alloy of complex structure by using first-principles simulations. Our initial focus is to reveal the detailed phase transition as well as the underlying mechanism. The most important is the difference in structural evolutions for both types of strain. On the other hand, the band structures at different strains are studied based on the Tran–Blaha modified Becke–Johnson (TB-mBJ) model potential,[16,17] to achieve the dependence of E_g on both types of strain, which is helpful in widening the technological applications with desired electronic functions in an ultraviolet-spectrum range.

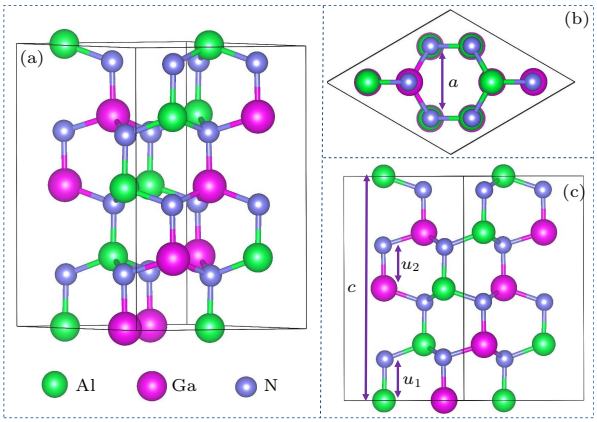

Fig. 1. Crystal structure of ground-state wurtzite alloy. Panels (b) and (c) are the schemes viewed along the [001] and [110] directions, respectively.

The total energy and band structure calculations are performed by using the projector augmented-wave method[19] as implemented in the VASP code.[20] The N $2s^22p^3$, Al $3s^23p$ and Ga $3d^{10}4s^24p$ orbitals

*Supported by the Fundamental Research Funds for the Central Universities under Grant No 2013QNA38.

**Corresponding author. Email: lixia@cumt.edu.cn

© 2016 Chinese Physical Society and IOP Publishing Ltd

are explicitly included as valence electrons. The electronic wave functions are described by using a plane wave basis set with an energy cutoff 650 eV. A Monkhorst–Pack k-point mesh of $4 \times 4 \times 4$ is used throughout the calculations to obtain well-converged results. The phonon-dispersion calculations are performed with the direct method implemented in the PHONOPY package.[21,22] This method uses the Hellmann–Feynman (HF) forces calculated for an optimized supercell through VASP. The $2\times2\times2$ supercell with 256 atoms is adopted for all phonon calculations with the accuracy of 0.05 THz for the highest optical zone-center frequency. The band structures are computed by using the TB-mBJ exchange potential, which in combination with the local density approximation (LDA)-correlation yields band gaps with an accuracy similar to hybrid functional or GW methods, but computationally less expensive.[16–18]

To better retain hexagonal symmetry, a $2 \times 2 \times 2$ 32-atom supercell is adopted to describe $Al_{1/2}Ga_{1/2}N$ alloy. Figure 1 shows that the bottom layer contains two AlN cells along the [110] direction and two GaN ones along the $[\bar{1}10]$ direction, while the upper consists of two AlN cells along the $[\bar{1}10]$ direction and two GaN ones along the [110] direction. To find out the strain-free lattice constants, the lattice vectors and atomic coordinates are fully relaxed until the HF force acting on each atom is reduced to less than 0.02 eV/Å. To examine the structural stability of the ground-state alloy, the phonon dispersion is computed by the finite difference method. As can be seen from Fig. 2, there are no imaginary phonon modes in the whole Brillouin zone, indicating that the structure is dynamically stable. In the presence of uniaxial (biaxial) strain (ϵ), relaxation is performed with the lattice constant c (a and b) fixed until the following conditions are satisfied within a small tolerance: $\sigma_{11} = \sigma_{22} < 0.02$ GPa ($\sigma_{33} < 0.02$ GPa) and $\sigma_{ij} = 0$ for $i \neq j$, where σ_{11} and σ_{22} are the stresses in the (0001) plane, and σ_{33} along the [0001] direction. Here σ_{33} (σ_{11}) is adjusted by changing ϵ_{33} (ϵ_{11}) step-by-step to reach all desired values.

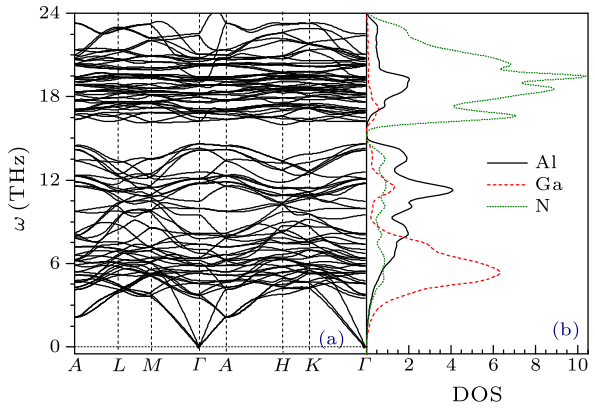

Fig. 2. Phonon-dispersion curves and PDOS of ground-state alloy.

In the presence of strain, a new lattice parameter corresponds to a specified uniaxial out-of-plane ϵ given by $\epsilon_{33} = (c - c_0)/c_0$ and a commensurate equibiaxial in-plane ϵ by $\epsilon_{11} = \epsilon_{22} = (a - a_0)/a_0$, where a_0 and c_0 are the strain-free lattice constants. Figure 3 shows the lattice-constant ratio c/a, internal parameters u_1, u_2, $u = u_1 + u_2$, and cell-volume $V - V_0$ as functions of uniaxial and biaxial ϵ, respectively. Figure 3(a) shows that c/a is greatly reduced by compressive ϵ_{33} and tensile ϵ_{11} until reaching ~1.20 for $\epsilon_{33} < -0.18$ and $\epsilon_{11} > 0.12$. Here u_1 (u_2) describes the relative positions of the nearest Al (Ga) and N atoms along the c-axis. Although u of AlN is larger than that of GaN, u_1 is always smaller than u_2. This is due to the fact that AlN displays the larger elastic constants, thus the larger bulk modulus than GaN, which leads to u_1 less sensitive to the change in chemical environments than u_2. Here u_1 and u_2 are drastically enhanced by compressive ϵ_{33} and tensile ϵ_{11} until reaching ~0.25, as shown in Fig. 3(b). The most important is that when $\epsilon_{33} < -0.18$ and $\epsilon_{11} > 0.12$, $u = u_1 + u_2 = 0.50$, as shown in Fig. 3(c), which is similar to the results of AlN and GaN.[9,10] This indicates that a higher-symmetry graphite-like structure with fivefold coordination is achieved and the structural details are displayed in Fig. 4, where an Al(Ga) atom bonds with the nearest two N atoms along the c-axis. It is noteworthy that c/a, u_1, u_2 and u change continuously at phase transition for ϵ_{33}, but discontinuously for ϵ_{11}, which leads to the similar behaviors in $V - V_0$. Since V represents the derivative of enthalpy $H = E + PV$ with respect to pressure P, where E and V are the alloying-cell energy and volume, respectively, the phase transition is of second order for uniaxial ϵ and of first order for biaxial ϵ.

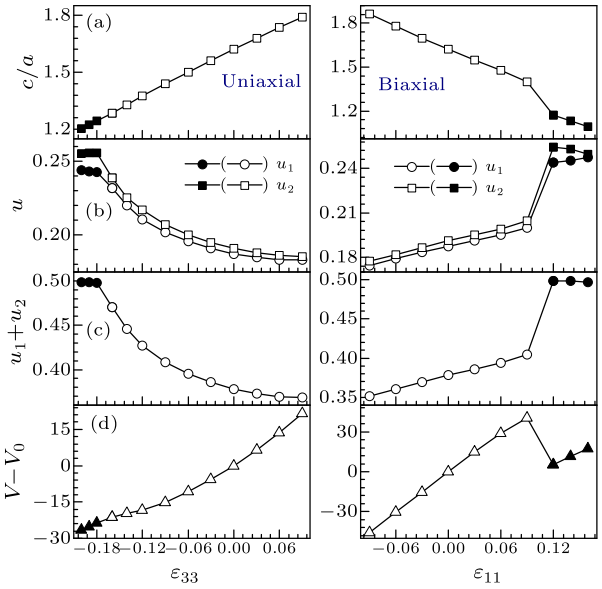

Fig. 3. Lattice-constant ratio c/a, internal parameters u_1, u_2, u_1+u_2 and supercell volume $V-V_0$ as functions of ϵ_{33} and ϵ_{11}, respectively. The phase transitions to a higher-symmetry structure occur at $\epsilon_{33} \cong -0.18$ and $\epsilon_{11} \cong 0.12$, respectively.

To reveal the underlying mechanisms of phase

transition, the energy derivative properties, such as elastic constants and phonon spectrums, are systematically investigated. Based on the Born stability criteria,[23] the independent elastic tensors c_{11}, c_{12}, c_{13}, c_{33} and c_{44} of stable hexagonal phase should satisfy $\triangle C = (c_{11}+c_{12})c_{33} - 2c_{13}^2 > 0$ and $c_{11} - |c_{12}| > 0$ and $c_{44} > 0$. Figure 5 shows $\triangle C$ and $c_{11} - c_{12}$ as functions of ϵ_{33} and ϵ_{11}, respectively. The positive $\triangle C$, $c_{11} - c_{12}$ and c_{44} indicate that the wurtzite phase remains mechanically stable for broad ranges of ϵ_{33} and ϵ_{11}. Furthermore, $\triangle C$ is reduced by compressive ϵ_{33} and tensile ϵ_{11} until becoming negative near the phase transitions, which are emphasized by the trends in $c_{11} - c_{12}$. Therefore, the mechanical instability plays a dominating role in the phase transition. On the other hand, $\triangle C$ of new phase remains positive for $\epsilon_{33} < -0.18$ and $0.11 < \epsilon_{11} < 0.15$, which means that the higher-symmetry structure can remain mechanically stable.

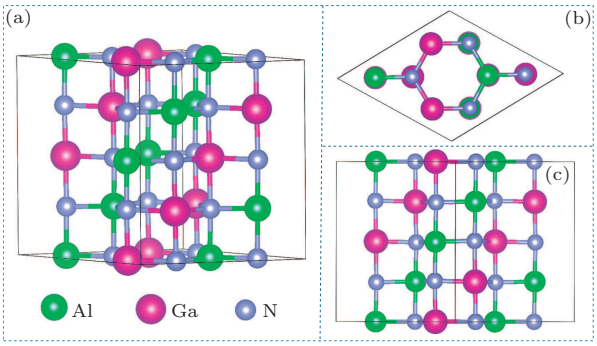

Fig. 4. Crystal structure of strain-induced high-symmetry alloy. Panels (b) and (c) are the schemes viewed along the [001] and [110] directions, respectively.

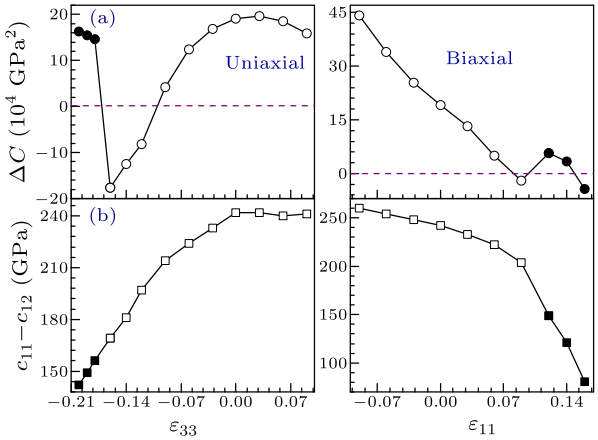

Fig. 5. Mechanical stability criteria ΔC and $c_{11} - c_{12}$ as a function of uniaxial and biaxial ϵ. The open symbols refer to the wurtzite phase and the solid ones to the new phase.

To reveal the evolutions of dynamic stability, the phonon dispersions at different ϵ are computed by the finite difference method. As can be seen from Fig. 6 that the phonon gap between transverse-optical (TO) and longitudinal-optical (LO) modes is observed for tensile ϵ_{33} and compressive ϵ_{11}, but not for compressive ϵ_{33} and tensile ϵ_{11}. The TO modes mainly originate from the vibrations of N atoms, the Ga atoms are responsible for the bottom part of LO modes and the Al atoms for the upper part of LO ones, which is attributed to the difference in atom mass. There are no imaginary phonon modes in the whole Brillouin zone in broad ranges of strain for wurtzite and higher-symmetry phases, which indicates that both phases can remain dynamically stable. The most important is that the phonon modes soften around the Γ point at phase transition for uniaxial strain, but not for biaxial strain. Therefore, the second-order phase transition is jointly driven by the mechanical and dynamical instability and the first-order transition only by the mechanical instability.

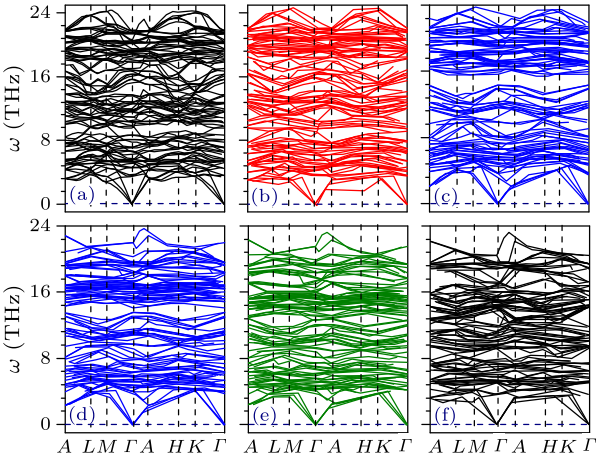

Fig. 6. Phonon-dispersion curves for different uniaxial and biaxial ϵ. Uniaxial: (a) $\epsilon_{33} = -0.18$, (b) $\epsilon_{33} = -0.16$ and (c) $\epsilon_{33} = 0.06$. Biaxial: (d) $\epsilon_{11} = -0.06$, (e) $\epsilon_{11} = 0.09$ and (f) $\epsilon_{11} = 0.12$. The crystal structures are higher symmetry in (a) and (f), and wurtzite in (b)–(e).

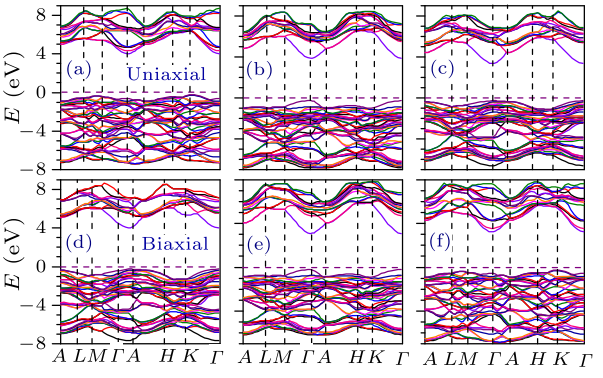

Fig. 7. TB-mBJ band structures at different ϵ. Uniaxial: (a) $\epsilon_{33} = -0.18$, (b) $\epsilon_{33} = -0.06$ and (c) $\epsilon_{33} = 0.06$. Biaxial: (d) $\epsilon_{11} = -0.06$, (e) $\epsilon_{11} = 0.06$ and (f) $\epsilon_{11} = 0.12$. The structures are higher symmetry in panels (a) and (f), and wurtzite in other panels. The Fermi level is set to zero in each panel.

The electronic structure is sensitive to the structural evolution,[24] where the coordination number increases to five from four. The band structures at different strains are shown in Fig. 7 in details. The wurtzite phase always keeps direct band struc-

ture, with the valence-band maximum (VBM) and conduction-band minimum (CBM) at the Γ (0,0,0) point, as shown in Figs. 7(b)–7(e). When the alloy is strain-free, the VBM states show a threefold degeneracy and are occupied by the N p_x, p_y and p_z orbitals, which is similar to the results of AlN and GaN.[9] More specifically, the VBM state of the wurtzite phase originates from the N p_z orbital for compressive ϵ_{33} and tensile ϵ_{11}, and from the N p_x and p_y ones for tensile ϵ_{33} and compressive ϵ_{11}. After the phase transition, E_g of the new phase is indirect, with the VBM at the K $(-1/3,2/3,0)$ point and the CBM at the Γ point, as shown in Figs. 7(a) and 7(f). Although the important contribution of the N p_z state to the VBM at the K point is observed, the repulsion between N p and Ga d_{z2} orbitals induces the indirect band structure. Figure 8 shows TB-mBJ E_g as functions of uniaxial and biaxial strains. The ground-state E_g of 4.24 eV is in good agreement with the HSE06 4.16 eV,[15] which indicates that the alloying configuration shows slight influence on E_g. The wurtzite phase shows different dependence of E_g on both types of strain. (1) The value of E_g is first enhanced and then reduced by compressive ϵ_{11}, with the maximum of 4.39 eV at $\epsilon \simeq -0.02$, but is always reduced by tensile ϵ_{11}. (2) The value of E_g is reduced by both compressive and tensile ϵ_{33}. The overall band-gap trend is attributed to the fact that the N p_z level is suppressed by compressive ϵ_{33} and tensile ϵ_{11} and the N p_x and p_y levels by tensile ϵ_{33} and compressive ϵ_{11}. It is noteworthy that the CBM state is always from the N s orbital. Similar to the difference in phase transitions, E_g of new phase increases with compressive ϵ_{33} and decreases with tensile ϵ_{11}. This is due to the different dependences of the VBM state on strain and should be helpful in widening the technological applications in an ultraviolet-spectrum range.

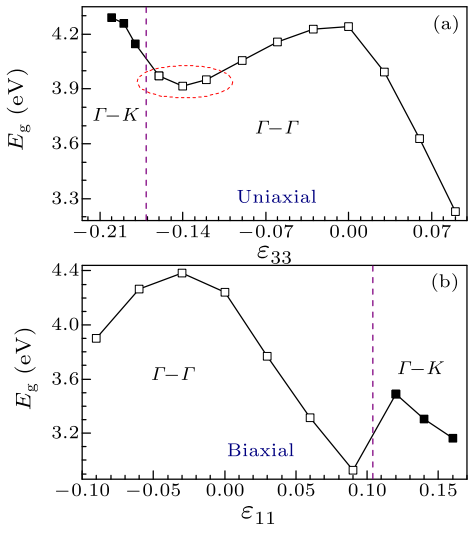

Fig. 8. TB-mBJ E_g as functions of uniaxial and biaxial ϵ. The open symbols refer to the wurtzite phase, and the solid ones to the new phase.

In summary, we have systematically investigated the effects of uniaxial and biaxial strains on the structural and electronic properties of $Al_{1/2}Ga_{1/2}N$ alloy of complex structure based on first-principles simulations. Although the higher-symmetry phases are energetically favorable and can remain stable, the second-order transition is driven by the mechanical and dynamical instabilities for uniaxial strain and the first-order transition only by the mechanical instability for biaxial strain. The band gaps of the wurtzite phase remain direct and those of new phase remain indirect. Furthermore, both types of strain can reduce the band gap before phase transition, while the band gaps are enhanced by uniaxial strain and reduced by biaxial strain after phase transition, which is attributed to the evolutions of valence states near the Fermi level with strain. This work will stimulate more investigations for semiconductor alloys to achieve desired electronic properties, thereby widening their technological applications with better performance.

We are grateful to the Advanced Analysis and Computation Center of China University of Mining and Technology for the award of CPU hours to accomplish this work.

References

[1] Vurgaftman I and Meyer J 2003 *J. Appl. Phys.* **94** 3675
[2] Wu J 2009 *J. Appl. Phys.* **106** 011101
[3] Yadav S, Sadowski T and Ramprasad R 2010 *Phys. Rev.* B **81** 144120
[4] Alahmed Z and Fu H 2008 *Phys. Rev.* B **77** 045213
[5] Xiao H, Li D, Li B and Dong H 2011 *Chin. Phys.* B **20** 067101
[6] Duan Y, Qin L, Tang G and Shi L 2008 *Eur. Phys. J.* B **66** 201
[7] Zhao B, Duan Y, Shi H, Qin L, Shi L and Tang G 2012 *Chin. Phys. Lett.* **29** 117104
[8] Dong L, Yadav S, Ramprasad R and Alpay S 2010 *Appl. Phys. Lett.* **96** 202106
[9] Duan Y, Qin L, Shi L, Tang G and Shi H 2012 *Appl. Phys. Lett.* **100** 022104
[10] Qin L, Duan Y, Shi H, Shi L and Tang G 2013 *J. Phys.: Condens. Matter* **25** 045801
[11] Yadav S and Ramprasad R 2012 *Appl. Phys. Lett.* **100** 241903
[12] Duan Y, Qin L, Shi L, Tang G and Shi H 2014 *J. Phys.: Condens. Matter* **26** 025501
[13] Madelung O 2004 *Semiconductors: Data Handbook* (Berlin: Springer)
[14] Duan Y, Li J, Li S and Xia J 2008 *J. Appl. Phys.* **103** 023705
[15] Duan Y, Lv D, Liu K, Wu H, Qin L, Shi L and Tang G 2015 *J. Appl. Phys.* **117** 045711
[16] Becke A and Johnson E 2006 *J. Chem. Phys.* **124** 221101
[17] Tran F and Blaha P 2009 *Phys. Rev. Lett.* **102** 226401
[18] Chen D, Huang M and Lu T 2006 *Chin. Phys. Lett.* **23** 943
[19] Blöchl P 1994 *Phys. Rev.* B **50** 17953
[20] Kresse G and Hafner J 1993 *Phys. Rev.* B **48** 13115
[21] Parlinski K, Li Z and Kawazoe Y 1997 *Phys. Rev. Lett.* **78** 4063
[22] http://phonopy.sourceforge.net
[23] Wu Z, Zhao E, Xiang H, Hao X, Liu X and Meng J 2007 *Phys. Rev.* B **76** 054115
[24] Duan Y, Qin L and Liu H 2016 *J. Phys.: Condens. Matter* **28** 205403